51st AIAA Aerospace Sciences Meeting including the New Horizons Forum and Aerospace Exposition
07 - 10 January 2013, Grapevine (Dallas/Ft. Worth Region), Texas

AIAA 2013-0325

An Investigation of the Irrotational Near Field of an Excited High-Speed Jet

Hind Alkandry[1], Michael Crawley[2], Aniruddha Sinha[3], Martin Kearney-Fischer[4], and Mo Samimy[5]
Gas Dynamics and Turbulence Laboratory
Aeronautical and Astronautical Research Laboratories
Department of Mechanical and Aerospace Engineering, The Ohio State University
2300 West Case Road
Columbus, OH 43235-7531 USA

The near-field pressure of a Mach 0.9 jet with Reynolds number of $6.2x10^5$ has been investigated to examine the response of the jet to low-frequency forcing with localized arc filament plasma actuators (LAFPAs). The well-defined actuation phase allows for the phase averaging of the near-field pressure in order to separate the relevant features of the response from the background turbulence. The resulting phase-averaged signal illustrates a compact wave with a positive pressure excursion preceding a negative one. This is indicative of a large-scale structure (a vortex ring) that is generated by each impulsively seeded perturbation. The signature of these large-scale structures is shown to rapidly decay with radial distance from the jet. Simultaneous measurements of acoustic far field were also performed along with the near field, allowing the relationship between them to be examined. Although the region near the jet shear-layer is largely hydrodynamic in nature, there is still significant correlation between the near-field pressure and the far-field acoustic around 30° polar angle, particularly as the jet evolves downstream past the potential core. This region is shown to shift upstream closer to the end of the potential core when the jet is forced.

Nomenclature

D	=	Nozzle exit diameter, m
U_j	=	Nozzle exit velocity (m/s)
f	=	Spectral frequency (Hz)
f_F	=	Forcing frequency (Hz)
Re_D	=	Reynolds number based on D and nozzle exit conditions
St_D	=	Spectral Strouhal number (fD/U_j)
St_{DF}	=	Forcing Strouhal number (f_FD/U_j)
p	=	Pressure, normalized by $\rho_j U_j^2$
p_{MS}	=	Mean square pressure
r	=	Radial coordinate normal to the jet axis (m)

I. Introduction

Jet noise has been an issue of enormous environmental, technological, and financial impact to both the civilian and military aircraft industry. The composition of jet noise and the relative strength of the noise sources are highly dependent on the jet temperature and Mach number. It is well established that there exists flow structures ranging in size from dissipation-scale to the order of the exit dimension of the jet nozzle. It is generally accepted that jet noise is produced by the interaction and disintegration of these structures[1]. In subsonic jets, the interaction and disintegration of flow structures produces what is known as mixing noise. A supersonic jet could also include screech tones, broad-bang shock associated noise, and Mach wave radiation. Various attempts have been made to manipulate the flow structures found in the shear layer (utilizing both active and passive control strategies) to reduce

[1] Graduate Research Associate, AIAA Student Member
[2] Graduate Research Associate, AIAA Student Member
[3] Postdoctoral Scholar at California Institute of Technology, AIAA Member
[4] Senior Aeronautical Engineer at Lockheed Martin Aeronautics, AIAA Member
[5] The Nordholt Professor of Mechanical and Aerospace Engineering, AIAA Fellow, Corresponding Author, samimy.1@osu.edu

the resulting noise with varying degrees of success. The purpose of this paper is to use active control on a subsonic jet to better understand the relationship between the irrotational pressure field (and thus the jet flow dynamics) and the radiated noise to the far field. Active control facilitates the study of the noise production mechanisms by isolating particular flow structures for study. Furthermore, forcing the jet provides a well-defined phase relationship allowing for phase-locked data acquisition for a better understanding of the jet dynamics.

Jet flow control is a well-researched topic with applications including, but not limited to, noise mitigation and mixing enhancement. Flow control methods can be divided into two basic categories: passive (geometrical modifications of the nozzle such as chevrons, lobed nozzles, etc.) [2-6] and active (modifiers which can be turned off to eliminate performance penalties when unneeded)[7-13]. Active flow control methods are desirable, but achieving control authority in high-speed and high Reynolds number flows is challenging.

Jets have three different instabilities, which have been well researched at low speeds and low Reynolds numbers[7-14]: the jet initial shear layer instability referred to as the Kelvin-Helmholtz instability, the jet column or jet preferred mode instability and, in the case of an axisymmetric jet, the azimuthal instability. More information on these instabilities and how they are relevant to the control of jets can be found in previous works [15, 16].

An important class of active flow control involves the excitation of flow instabilities. One or more of the flow instabilities mentioned above might be manipulated in order to actively control jets. As the speed and the Reynolds number of the jet increase, so do the background noise, the instability frequencies, and the flow momentum. The relatively few previous attempts at active flow control of highly energetic jets have used acoustic drivers to control high subsonic jets around their preferred mode[17-19]. Unfortunately, acoustic drivers lose control authority in these highly energetic jets at high Reynolds numbers (typically up to 100,000). In order to operate in this environment, actuators must provide excitation signals with much higher amplitudes and frequencies.

Localized arc filament plasma actuators (LAFPAs) have been developed and implemented for active control of jets at The Ohio State University over the past several years. The Gas Dynamics and Turbulence Laboratory (GDTL) at The Ohio State University has used these actuators for noise mitigation and flow control in a large range of Mach numbers and temperatures[15, 16, 20-24]. Each LAFPA consists of a pair of electrodes placed very near the nozzle exit, connected to a high voltage source through a switching circuitry. Closing the switch causes the voltage across the electrodes to rise until breakdown of the air between them occurs, which introduces perturbations to the flow. These perturbations excite the flow instabilities. Significant control authority on these flows has been demonstrated using LAFPAs with the aid of various measurement techniques (particle image velocimetry, schlieren imaging, flow visualization, and acoustic measurements in the flow-field, intermediate field, and far field). Furthermore, previous investigation techniques have revealed that forcing with LAFPAs has the effect of organizing the jet shear layer[20, 22, 23, 25]. This means that large-scale structures are created in the flow with periodicity (in both time and azimuth) closely matching the excitation.

The irrotational near-field pressure has also been examined (both by GDTL and by other researchers in literature)[26-29], but not as extensively as the jet flowfield and acoustic far field mentioned above. The goal of the present study is to use near-field pressure measurements to further characterize the effect of LAFPA forcing on jets and to better understand the jet dynamics associated with the radiating noise. The near-field pressure consists of both hydrodynamic and acoustic signals. The acoustic signal is the propagative part of the pressure signal while the hydrodynamic pressure is characterized by exponential decay of these fluctuations with increasing radial distance[30, 31]. Furthermore, the hydrodynamic field contains the convective signature of the large-scale structures in the shear layer. The near-field pressure probes afford a non-intrusive measurement, as the probes do not impinge into the shear layer. The earlier work[29] was an initial validation of our hypothesis that large-scale structures are generated with regularity by the impulsive forcing, so that even at very low frequencies of forcing we can discern them clearly in the phase-averaged near-field pressure. These pressure perturbations could be explained by *linear* parabolized stability equations. Structure interaction was shown to set in when the forcing frequency approaches the jet column mode frequency, but a quasi-linearity was observed in the interactions for frequencies somewhat beyond the jet column mode. In this article, an extension of the above study is reported. Specifically, the region of the near field measured is significantly enlarged. Moreover, the far field acoustics are acquired simultaneously. Finally, extensive correlation studies are conducted to investigate the details of noise propagation within the near field, and from the near field to the far field.

II. Experimental Setup

All experiments are conducted in the newly upgraded anechoic chamber at the GDTL within the Aeronautical and Astronautical Research Laboratories (AARL) at The Ohio State University. A schematic of the chamber is illustrated in Figure 2. The design and validation of the chamber has been documented in detail[32]. The compressed

air, supplied with three 5-stage reciprocating compressors, is filtered, dried, and stored in two cylindrical tanks with a volume of 43 m^3 and pressure up to 16 MPa. The compressed air is passed through a storage heater at a set temperature to heat the air to the desired temperature (the heater was not utilized in the current work), and then supplied to the stagnation chamber of the jet facility. The air is discharged horizontally through the nozzle into an anechoic chamber and then through an exhaust system to the outdoors. The present work employs a stainless steel, axisymmetric, converging nozzle with an exit diameter of 25.4 mm (1 in.). The nozzle is operated at a hydrodynamic Mach number of 0.9 with a Reynolds number based on jet diameter of approximately 6.2×10^5.

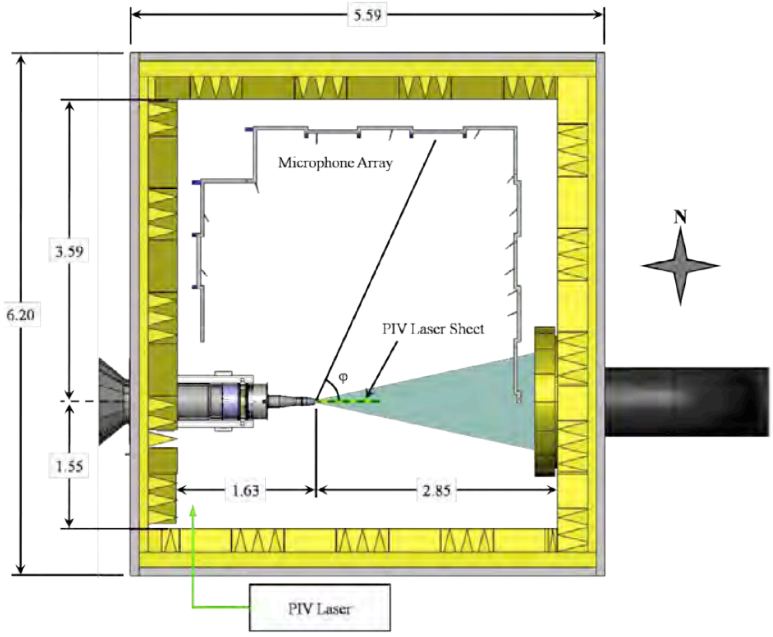

Figure 2. Schematic of anechoic chamber and jet.

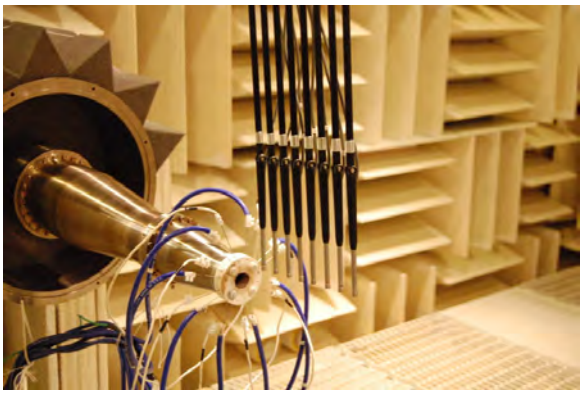

(a)

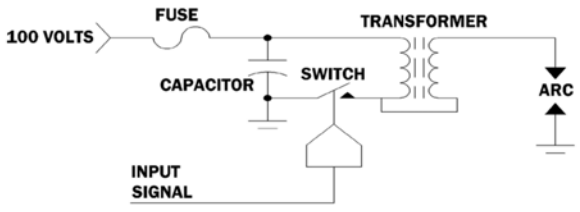

(b)

Figure 1.(a) A photograph of anechoic chamber and jet showing LAFPAs housed in nozzle extension and linear array for pressure measurements. (b) Schematic of high-voltage circuitry for one LAFPA channel.

A. Localized Arc Filament Plasma Actuators

As mentioned, flow control actuators known as localized arc filament plasma actuators have been developed in-house at the GDTL. Each actuator consists of a pair of pin electrodes. Tungsten rods, with a diameter of 1 mm, are utilized as the electrodes. The electrodes are distributed around the nozzle extension perimeter, approximately 1mm upstream of the nozzle exit plane, as shown in Figure 1(a). Measured center-to-center, the spacing between a pair of electrodes for each actuator is 4 mm, and the distance between the neighboring electrodes of two adjacent actuators is 6 mm. The electrodes are held in place by a nozzle extension made of boron nitride. A ring groove of 0.5 mm depth and 1 mm width cut into the extension is used to house the electrodes and to shield the plasma[33]. With this arrangement, eight actuators are uniformly distributed around the nozzle extension so that the azimuthal spacing between two adjacent actuators is 45°.

A second-generation multi-channel high voltage power supply and plasma generator, designed and built at The Ohio State University, is utilized to power the plasma actuators. The plasma generator enables simultaneous powering of up to eight LAFPAs with independent frequency, duty cycle/pulse width, and phase control of individual actuators. Each individual circuit consists of a switchable capacitor in line with a high voltage transformer; the arcing electrodes are connected to the secondary side of the coil. The capacitor is charged by a 100 V DC power supply when the first switch is closed and the second is open; at the user-specified time the switches flip and it discharges through the coil. A schematic of the circuitry can be found in Figure 1(b). The switches are controlled by a 16-channel digital I/O card and National Instruments' LabVIEW software, operated by a dedicated computer. The pulse width was held constant at 7 μs, which was found to be the minimum pulse width at which the actuators consistently arced for all frequencies explored in this study[33]. This cycle can repeat to a maximum of 100,000 times per second (100 kHz), though presently it is limited to only 20 kHz by cooling requirements.

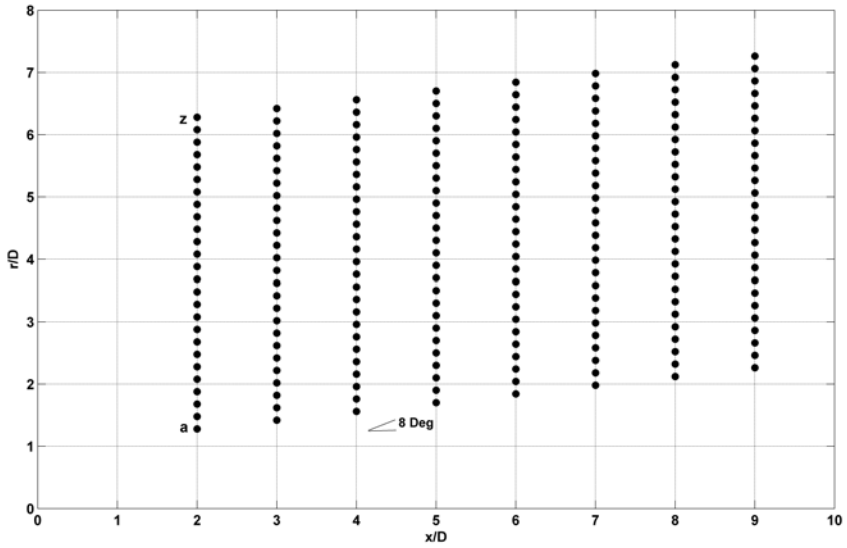

Figure 3. Microphone array grid coordinates for irrotational pressure field measurements

B. Data Acquisition

1. Near-Field and Far-Field Pressure

The irrotational pressure field is acquired using a linear array of eight microphones in a meridional plane of the jet (see **Figure 1**(a)). The linear microphone array is attached to a linear traverse and a rotation mount, both of which can be independently controlled. The separation between any two microphones is 25.4 mm (1 in). For the present experiment, the most upstream microphone is placed at $x/D = 2$, measured from the nozzle exit plane. The linear array is rotated such that the tips of the microphones form a line inclined at 8° to the jet axis. The initial radial location of the most upstream microphone is $r/D = 1.28$. This configuration ensures that the sensors are approximately equidistant from the outer edge of the shear layer of the unforced Mach 0.9 jet, as measured in earlier

PIV experiments[21]. In the subsequent runs, the microphones are shifted in the radial direction in 5.08 mm (0.2 in.) increments for a total travel of $r/D = 5$. A schematic of the microphone placements used is presented in **Figure 3**.

Far-field acoustic pressure was simultaneously acquired at eleven polar angles spanning 25° to 120°, as measured from the downstream jet axis. The far-field microphone array is comprised of two linear sections running perpendicular to the jet axis that contain the upstream and downstream angle microphones, and a third linear section running parallel to jet for the sideline angle microphones (Figure 2). The microphones are oriented such that the normal vector from their tips intersects the jet downstream axis at the nozzle exit. The radial distance of the microphones ranges from 96.5D at 25° to 145D at 60°.

The microphones used are ¼ inch Bruel & Kjaer (B&K) 4939. The voltage signal from each microphone is band-pass filtered from 20 Hz to 100 kHz, amplified by B&K Nexus 2690 conditioning amplifiers, and simultaneously acquired using National Instruments PXI-6133 A/D boards and LabVIEW software. The microphones are calibrated using a 114 dB, 1 kHz sine wave, and the frequency response of the microphones is flat up to 80 kHz with the microphone grid cover removed. Signals are acquired at 200 kHz with 81920 data points per block of samples. Ten such blocks of data are recorded for each experimental case producing a total sample time of about 4 seconds.

In this study, the jet is excited at a forcing frequency, in terms of Strouhal number, of $St_{DF} = 0.02$. This low forcing frequency was chosen such that the large-scale structures generated are convected downstream without any interaction with the subsequent or previous structures. The eight LAFPAs are operated in phase to simulate axisymmetric forcing ($m = 0$).

2. *Phase Averaging*

The phase averaging technique used by Sinha et *al.*[29] is employed in order to study the evolution of the seeded perturbations. The actuators have control authority on the jet so that forcing results in a highly correlated fluctuation field – thereby justifying the application of phase averaging. Since the frequency and firing order of the actuators are specified by the user and held fixed by the controlling computer throughout an experiment, the only unknown information is the instantaneous phase. The pulse train controlling the first LAFPA is supplied to an arbitrary waveform generator (Agilent 3320A 20 MHz), where the rising edge on the transistor-transistor logic (TTL) pulse triggers a rising ramp signal over a time interval which is shorter than the forcing period. This ramp signal is acquired simultaneously with the near- and far-field pressure signals using the National Instruments hardware and LabVIEW program. This ramp signal is necessary in order to locate the zero phase of the actuator signal to sub-sample accuracy and to ensure that the short duration plasma pulses (7 μs) can be robustly identified in potentially noisy data. Utilizing the known phase information, the pressure signals can be phase averaged to examine consistently occurring signal features.

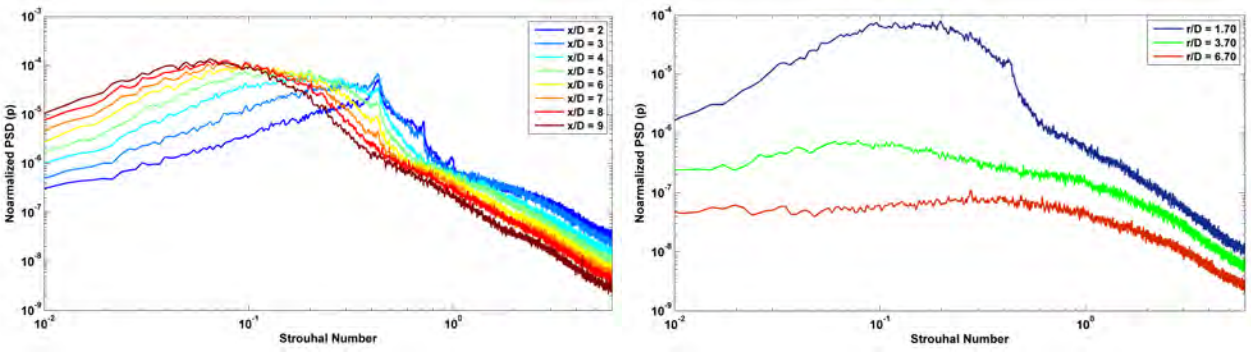

(a) **(b)**

Figure 4. Power spectral density for unforced jet: (a) PSD for first array position at various axial locations, (b) PSD at $x/D = 5$ for three radial locations.

III. Results

A. Unforced Jet

A characterization of the near-field pressure in the unforced jet situates the subsequent discussion of the impulse response. The power spectral density (PSD) plots for the unforced jets are presented in Figure 4. The PSD is normalized by the jet dynamic head $\rho_j U_j^2$, where ρ_j is the jet exit density and U_j is the jet exit velocity. This scaling is the established normalization for the near-field pressure fluctuation amplitude for cold subsonic jets[30, 31]. The frequency is converted to the non-dimensional Strouhal number $St_D = fD/U_j$. Figure 4(a) illustrates the PSD for the first measured microphone array position (label (a) in Figure 3). As shown in Figure 4(a), increasing the axial distance leads to an overall shift of the peak towards lower Strouhal numbers. This behavior has been noted by previous researchers, and associated with the growth of large-scale structures in the shear layer[30]. Figure 4(b) shows the spectra for multiple radial locations at the same axial location (x/D = 5). Previous research has shown that hydrodynamic fluctuations decay exponentially, while acoustic fluctuations decay algebraically[30], so it can be inferred that the much stronger decay of the spectral peak in Figure 4(b) is an indication of hydrodynamic fluctuation decay. Along the first array location (location (a) in Figure 3), the pressure field is dominated by hydrodynamic fluctuations, whereas the acoustic component is more dominant at the last array location ((z) in Figure 3). A quick note must be made regarding the narrowband tones observed in the most upstream microphones in Figure 4(a). Similar tones have been observed previously in our facility (though this was not always repeatable), and were suspected to be the result of a minor acoustic resonance in the jet plumbing. Given that the tones are of relatively low amplitude, decay quickly as the jet evolves downstream, and are not observed in the far-field spectra, it is believed that our results are unaffected by their presence.

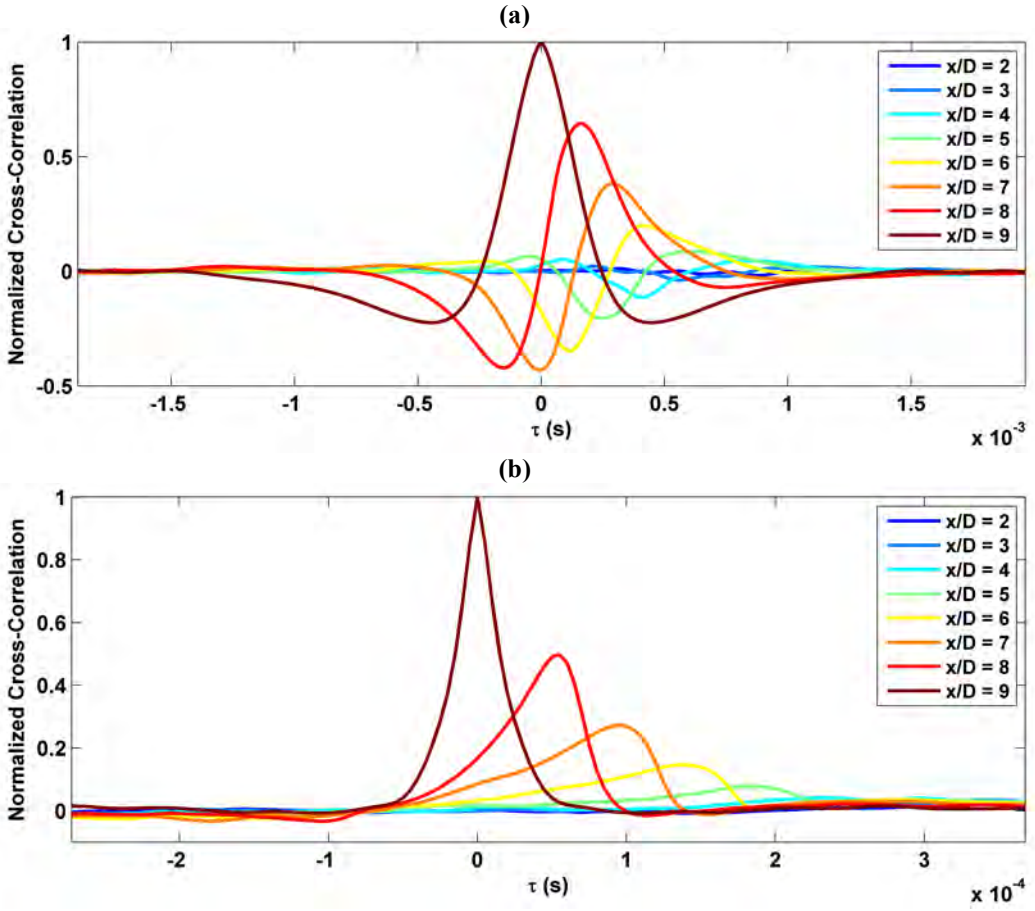

Figure 5. Normalized cross-correlations of the near-field pressure fluctuations with the reference microphone at x/D = 9: (a) First array location, (b) Last array location.

Space-time correlation characteristics of the jet are investigated in order to gain insights into the physical mechanisms that lead to generation and radiation of noise due to turbulent mixing in jets. The normalized cross-correlations of the near-field pressure with the reference microphone at $x/D = 9$ (last microphone in the array) are presented in Figure 5. The normalization is such that the autocorrelations at zero lag are identically 1.0. Figure 5(a) illustrates the first radial location where the pressure field is dominated by hydrodynamic fluctuations. Little correlation is observed when the microphone is placed greater than 5D from the reference microphone. The correlation increases with decreasing streamwise distance reaching a maximum of approximately 0.63 when the sensor is 1D from the reference microphone. Although not shown in this paper, similar correlations were acquired for various reference microphones and similar levels of correlation were observed. Slightly lower maximum correlation values are observed for the last array position (Figure 5(b)). Furthermore, note nearly an order of magnitude change in the time lag. One of the major differences between the two array locations presented is that there are no strong negative excursions for the last array location. Additionally, the width of the positive excursion is broader in the case where the array is near the shear layer (array location (a) in Figure 3). These dissimilarities can be observed between the autocorrelation functions as well ($x/D = 9$). The autocorrelation for the last array position (Figure 5(b)) lacks any significant negative excursions. As expected, as the sensor is placed away from the reference microphone similar correlation shape is observed with progressively lower amplitude.

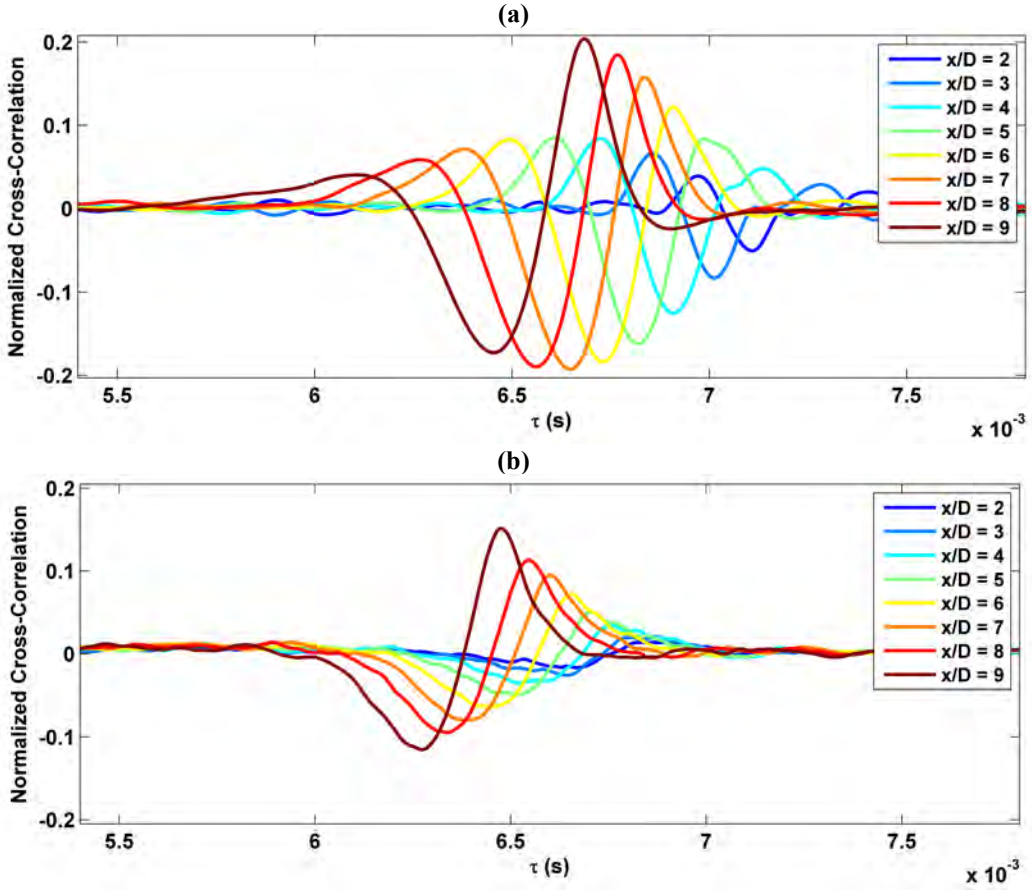

Figure 6. Normalized cross-correlations of the near-field pressure fluctuations with the 30° far-field microphone: (a) First array location, (b) Last array location.

The variation of the normalized cross-correlations of the near-field pressure along the first array position and last array position with the far-field microphone at 30° are shown in Figure 6(a) and (b), respectively. As is evident from Figure 6(a), the correlation increases as x/D increases and the structures in the jet evolve, reaching a maximum of roughly 0.2 at $x/D = 9$, which is the last microphone location in the array. This is consistent with previous researchers who have shown that the correlations are strongest downstream of the end of the potential core[34,35], which occurs at roughly $x/D = 6$ for this jet[21]. Given that the maximum correlation is occurring at the end of the

measurement window, this metric should be further evaluated by extending the measurements further downstream, which will be examined in future studies. In addition to the maximum amplitude, the shape of the correlations evolves as the microphones are traversed downstream, which is more clearly illustrated in Figure 8 for the first array position. For example, at x/D = 5.0 (Figure 8), the correlation curve is roughly symmetric: it has one large amplitude negative peak, bookended by two lower amplitude positive peaks (similar to the shape of the Mexican hat wavelet). Upstream of this position, the earlier positive peak has greater amplitude than the later one, while downstream of this position the later positive peak is dominant and the negative peak starts to gradually decrease. This trend in the shape of the correlation for the first array position is dissimilar to the last array location in that there is a sustained growth for both the positive and negative excursions (Figure 6(b)). Additionally, the last array location reaches a maximum of roughly 0.15, which is less than that observed in Figure 6(a).

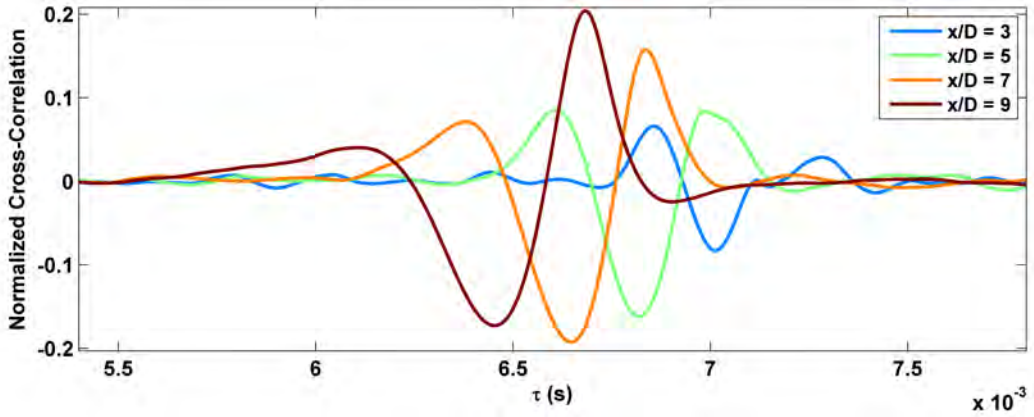

Figure 8. Normalized cross-correlation of the near-field pressure fluctuations with the 30° far-field microphone for the first array location.

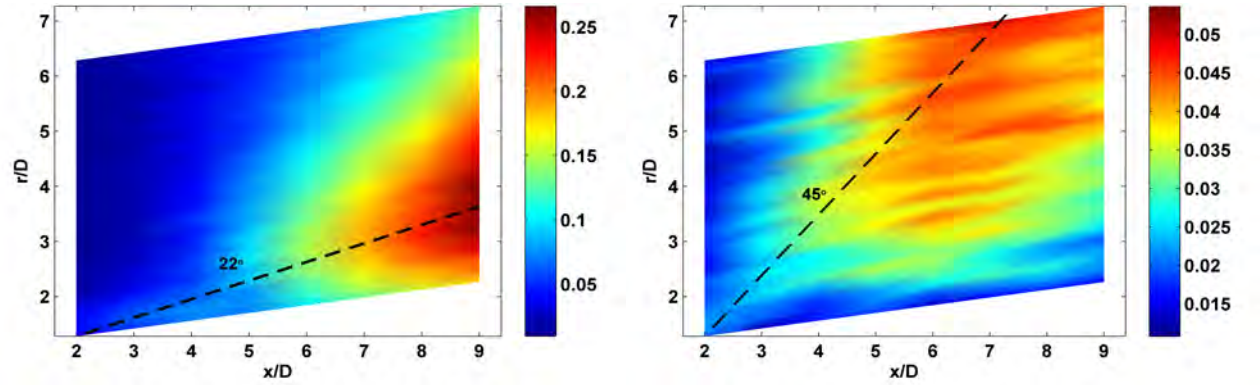

(a) **(b)**

Figure 7. Maximum normalized cross-correlation of the near-field pressure fluctuations: (a) with 30° far-field microphone, (b) with 60° far-field microphone.

In Figure 7, the maximum cross-correlation values between the near-field microphone signals and the far-field microphone signal at a given polar angle are plotted as a function of spatial coordinates of the near-field microphones. The maximum correlation is clearly a function of both axial and radial positioning of the near-field microphone. For the upstream microphone positions, particularly at large radial distances, the maximum correlation to 30° far field (Figure 7(a)) is virtually zero. This is expected given that the acoustics associated with the large-scale structures have been shown to radiate predominantly to the downstream angles[1]. The greatest correlation values are observed in the downstream direction, at an approximate angle of 22° with respect to the jet exit. It is to be noted that this angle is dependent on the chosen viewing window and therefore is not an absolute number.

Compared to the correlations at 30°, the correlations to 60° (Figure 7(b)) are of significantly lower amplitude, and peak at a higher angle (approximately 45°). This is consistent with the concept that the largest contribution to the sideline angles is due to small scale, high frequency fluctuations, in contrast to the downstream angles, which are associated with large-scale structures. The region of high correlation relative to its surroundings is much broader at this polar angle than at 30°. The most upstream region has very low correlation to the acoustic far field at 60° (again, as expected), however in this case the region close to the jet shear layer also shows low correlations to the 60° far-field microphone.

B. Forced Jet

The forcing response of the jet is characterized using the near-field pressure measurements. The linear array of near-field probes is held fixed at the locations mentioned earlier. The forcing frequency is normalized to the forcing Strouhal number $St_{DF} = f_F D/U_j$.

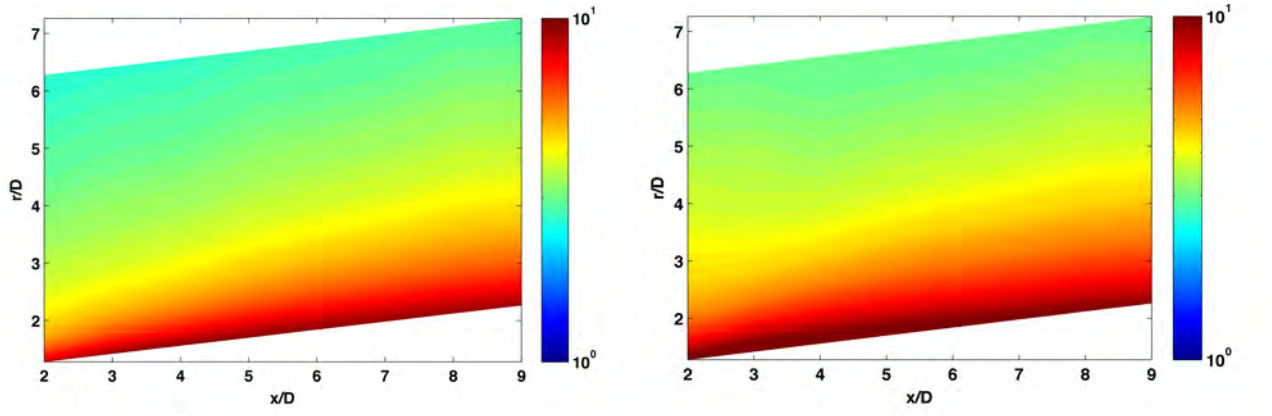

Figure 9. Mean-square of near-field pressure fluctuations: (a) Unforced jet, (b) Forced jet (St_D = 0.02).

1. Time-averaged response

The simplest metric of the time-averaged response of the near-field pressure is the mean square (or equivalently, variance) of the pressure fluctuations, p_{MS}. The p_{MS} in the unforced jet for the entire x-r domain is presented in Figure 9. It should be noted that the data is presented in a log scale. The growth and decay of the near-field pressure amplitude with axial distance has been well-documented[27, 36, 37]. The near-field pressure is primarily hydrodynamic at the array locations closest to the shear layer. Thus, the behavior of p_{MS} in the region closest to the shear layer is indicative of the corresponding dynamics of the large-scale structures that are evolving downstream. Furthermore, the near-field pressure amplitude rapidly decreases with increasing radial distance (Figure 4(b)), this is further shown by the behavior of p_{MS}. Forcing the jet at a St_{DF} = 0.02 (Figure 9(b)) causes the growth and decay of the near-field pressure amplitude to move upstream closer to the nozzle exit with a maximum between x/D = 2.5 to 5.5. This is consistent with the concept that each actuator impulse is creating a flow perturbation which develops into a large-scale structure that convects downstream[29].

2. Phase-averaged response

The main interest in the present analysis is the new information that the simultaneous acquisition of the actuation phase provides. The following figures represent the phase-averaged pressure response at each microphone for forcing the axisymmetric mode at St_{DF} = 0.02 (corresponding to a frequency of approximately 250 Hz).

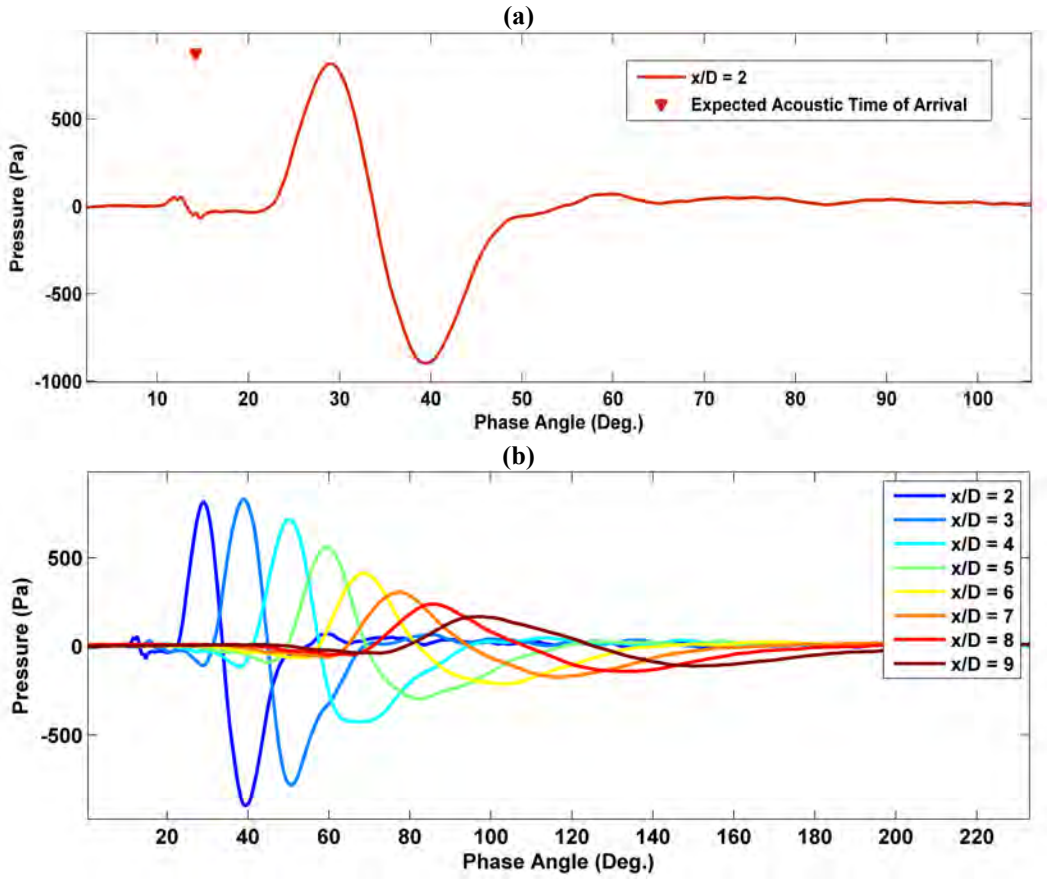

Figure 10. Phase-averaged waveform: (a) *x/D* = 2 and *r/D* = 1.28, (b) First array position.

Figure 10 shows the phase-averaged pressure results for the first array position that is just outside of the shear layer. The most upstream microphone in this array position (Figure 10(a)) is located at *x/D* = 2 and *r/D* = 1.28. As can be seen in Figure 10(a), each actuation pulse generates two well-defined waves (in the case of the first microphone, the positive peaks of the two waves occur at phase angles of approximately 12° and 29°), both with a positive excursion preceding a negative excursion. The first wave has smaller amplitude and arrives at the microphone much earlier. The triangular marker displayed in Figure 10(a) represents the expected time of arrival at the microphone of an acoustic wave travelling at the ambient speed of sound leaving the nozzle origin at zero phase. This expected time-of-arrival lines up fairly well with the first compact wave in the upstream microphone, suggesting an acoustic phenomenon. Given these observed characteristics in addition to previous characterizations performed in Sinha et *al.*[29], this wave is understood to be the noise of the plasma breakdown travelling directly without being modified by the jet, i.e. actuator self-noise. The actuator self-noise dissipates quickly, becoming indistinct after the phase-averaging process at the downstream microphones (Figure 10(b)). The second compact wave generated by each actuation is much stronger and is representative of the hydrodynamic response of the jet (i.e. the signature of the large-scale structures)[29]. Lastly, these pressure fluctuations appear to dissipate with increasing axial distance as has been previously shown[29].

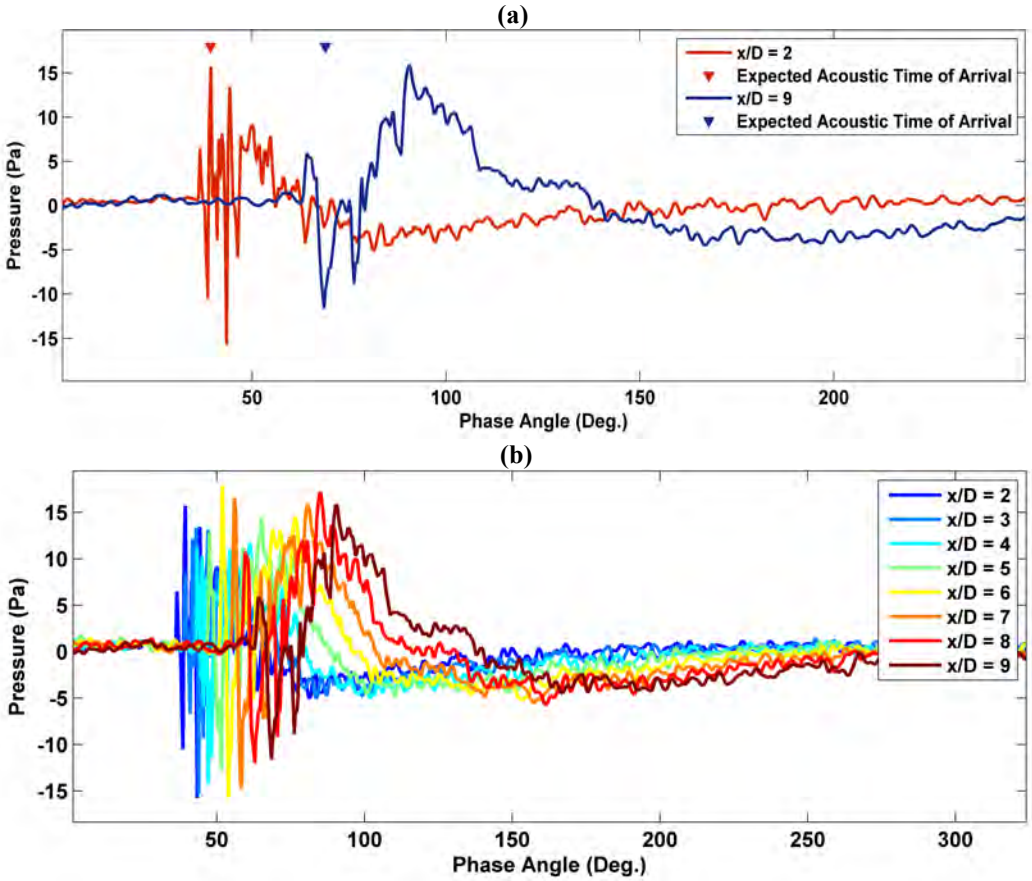

Figure 11. Phase-averaged waveform: (a) *x/D* = 2 and *9* for the last array position, (b) Last array position.

The phase-averaged waveform for the last radial position (z in Figure 3) is presented in Figure 11. Note over an order-of-magnitude scale change in the ordinates of Figure 10 and Figure 11. In this array position, the most upstream microphone is at $x/D = 2$ and $r/D = 6.28$ (Figure 11(a)). The expected time-of-arrival lines up fairly well with the first large amplitude wave over the entire axial extent indicating that this primary feature is actuator self-noise. Furthermore, this suggests that the array is no longer in the hydrodynamic field and thus does not capture the convective signature that is due to the large-scale structures in the shear layer. Unlike the first array location (Figure 10) where the second wave constitutes a positive excursion followed by a negative one, the latter array location constitutes mainly a positive excursion.

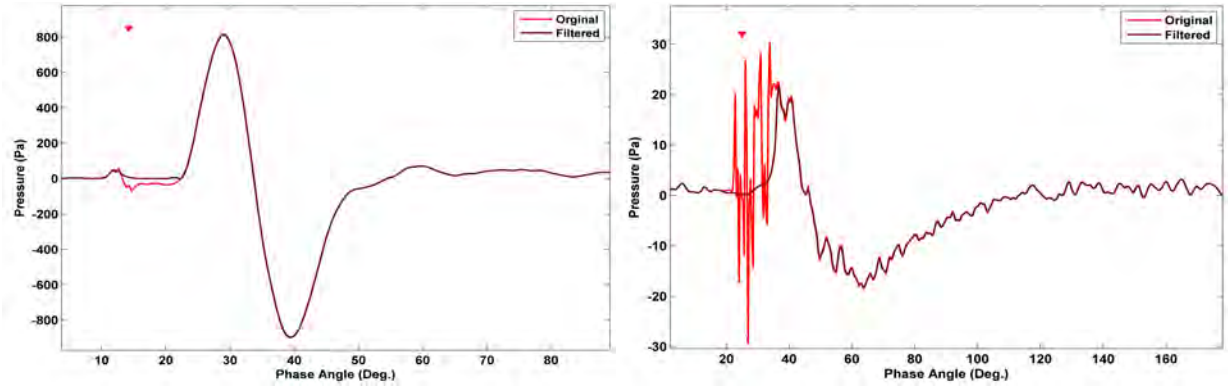

Figure 12. : Phase-averaged waveforms for the original and filtered waveforms at (a) *x/D* = 2.0, *r/D* = 1.28, (b) *x/D* = 2.0, *r/D* = 3.68.

Figure 12 shows the phase-averaged waveforms at two radial positions (r/D = 1.28 and r/D = 3.68) for the most upstream microphone. The first perturbation in each case is observed to align well with the expected time-of-arrival for an acoustic wave traveling directly from the actuators to the microphones as previously discussed. For radial positions close to the jet shear layer, as in Figure 12(a), the near-field pressure signal is dominated by the hydrodynamic response of the jet. Here the actuator-self noise is producing an almost negligible amount of fluctuation, as was also shown in Figure 10. However, due to the relatively slow decay of the acoustic component in comparison to the more rapid decay in hydrodynamic fluctuations, as the microphone is traversed outwards, the actuator-self noise begins to represent a significant contribution to the overall intensity of the signal. Additionally, as in Figure 12(b), the arrival of the actuator self-noise begins to coincide with that of the signature of the large-scale structures obscuring the near-field response and making analysis techniques, such as cross-correlations, difficult to interpret. Even though the speeds of the two signals are quite different, this occurs because of the significant differences between the distances the two signals must travel to get to the microphone. Therefore, it is necessary to apply a filter to the phase-averaged waveforms to remove the actuator self-noise.

The filtering algorithm consists of a continuous wavelet transform applied to both the phase-averaged response and the instantaneous pressure signals. The 4th-order Paul wavelet is one of the most suitable wavelets available among the numerous mother wavelets. The similarity of the imaginary part of this mother wavelet with the phase-averaged response is particularly notable[29]. In the wavelet domain the actuator self-noise produces high frequency oscillations, which can be filtered out via a smoothing operation (i.e. moving average). After smoothing in the wavelet domain, the waveform is transformed back into the temporal domain where it then undergoes another smoothing operation in order to remove any small oscillations that were introduced into the signal during the reconstruction. As can be seen in Figure 12, the near-field hydrodynamic signal is unaffected by the filtered algorithm, whereas the actuator self-noise has been almost entirely removed. Unless otherwise mentioned, the wavelet filter will be applied to all pressure signals hereafter.

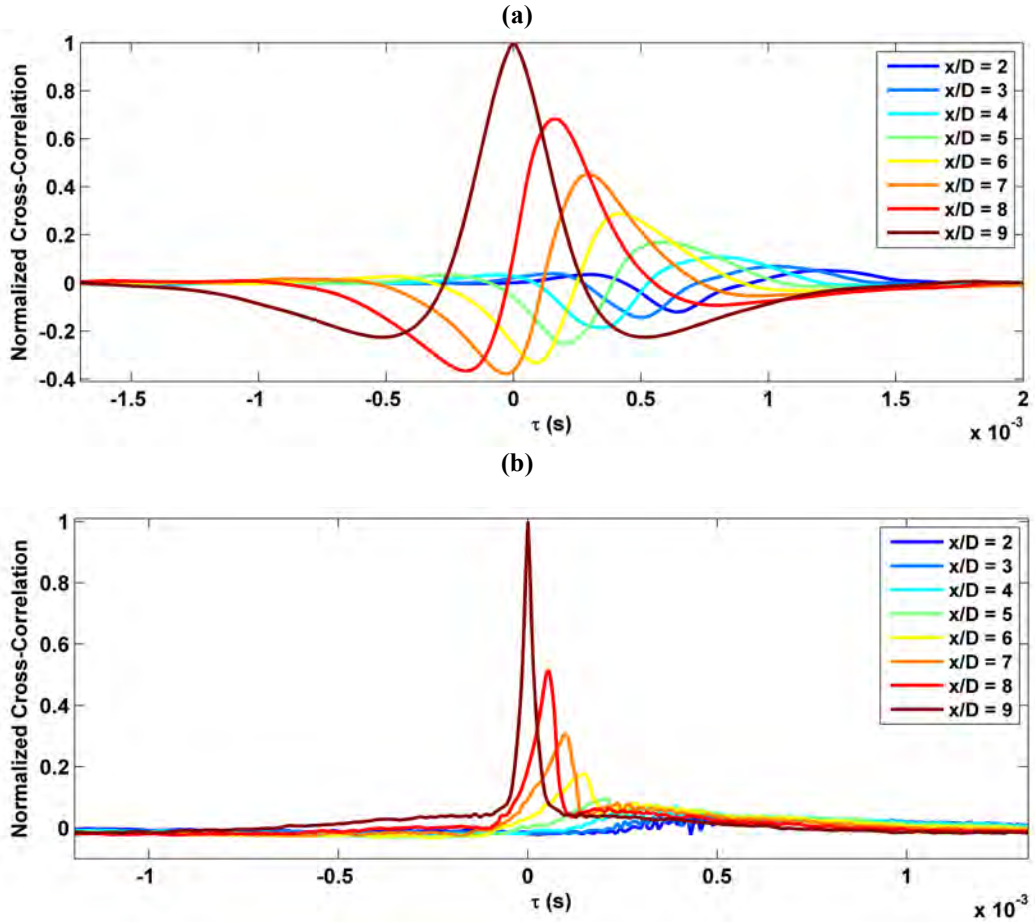

Figure 13. Normalized cross-correlations of the forced instantaneous near-field pressure with the reference microphone at x/D = 9: (a) First array location, (b) Last array location.

The normalized cross-correlations and autocorrelation of the instantaneous near-field pressure for the forced jet with the reference microphone at $x/D = 9$ (similar to Figure 5) are presented in Figure 14. Note that the scale (level and range) is varied between Figure 13(a) and (b) in order to better examine the trends observed. Unlike Figure 5(a) where roughly no correlation is observed for the upstream microphones in the first array location, correlation (although small) is visible over the entire axial extent for the forced jet. Furthermore, the correlation shape is highly similar to that observed for the unforced jet (Figure 5(a)). The positive peak observed for the last array in the unforced jet (Figure 5(b)) however, has a broader width than that seen in the forced case. This difference can also be observed for the autocorrelation function ($x/D = 9$).

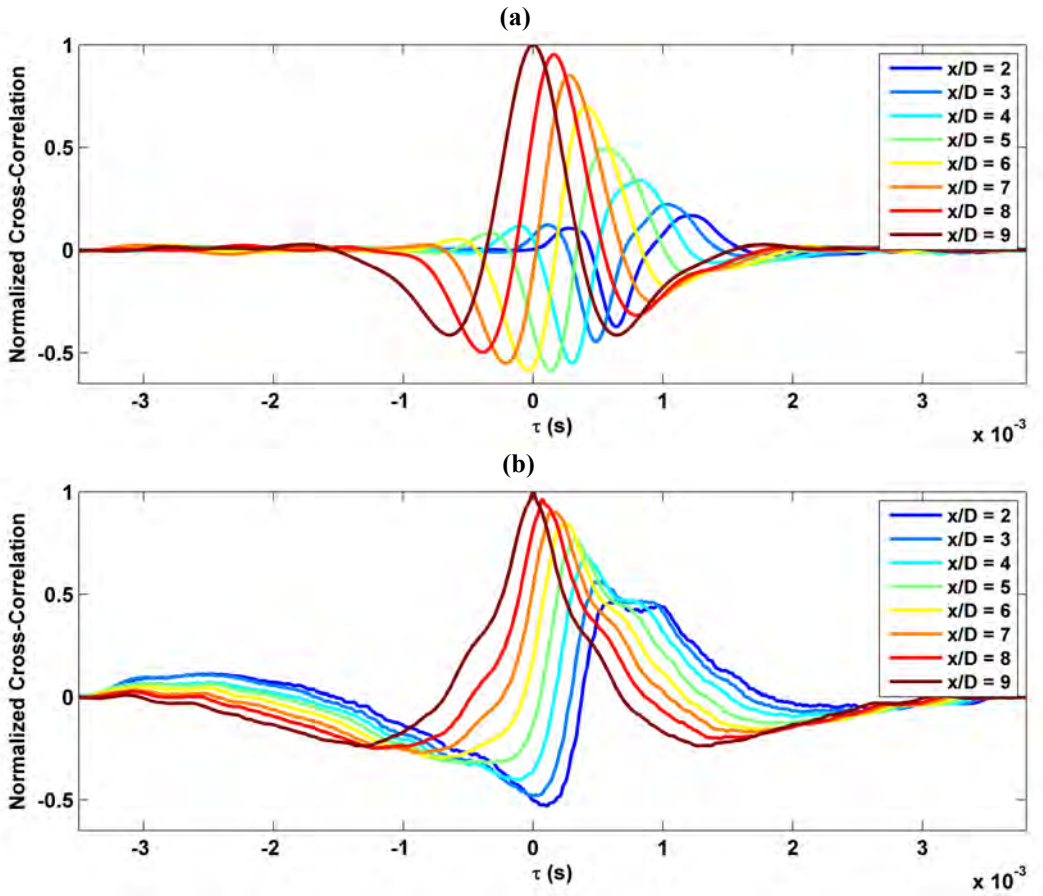

Figure 14. Normalized cross-correlations of the phased-averaged waveforms with the reference microphone at $x/D = 9$: (a) First array location. (b) Last array location.

The normalized cross-correlations of the phase-averaged waveform for the forced jet with the reference microphone at $x/D = 9$ (similar to Figure 5) are presented in Figure 14. Once again, correlation is noticeable over the entire axial extent for the forced jet, even with quite large distances. Furthermore, as the probe is placed closer to the reference microphone the shape of the correlation resembles that of the autocorrelation, as is expected. As the probe is placed closer than $4D$, a second negative excursion following the positive is observed similar to the autocorrelation. However, this is not the case in the instantaneous forced jet (Figure 13(a)) where the cross-correlations consist of simply a negative excursion preceding a positive. Lastly, the correlation shape of the last array position (Figure 14(b)) is initially roughly symmetric with the negative excursion rapidly decreasing as the jet evolves downstream. This is dissimilar to the unforced jet (Figure 5(b)) and the instantaneous forced signals (Figure 13(b)) where no negative excursions are observed.

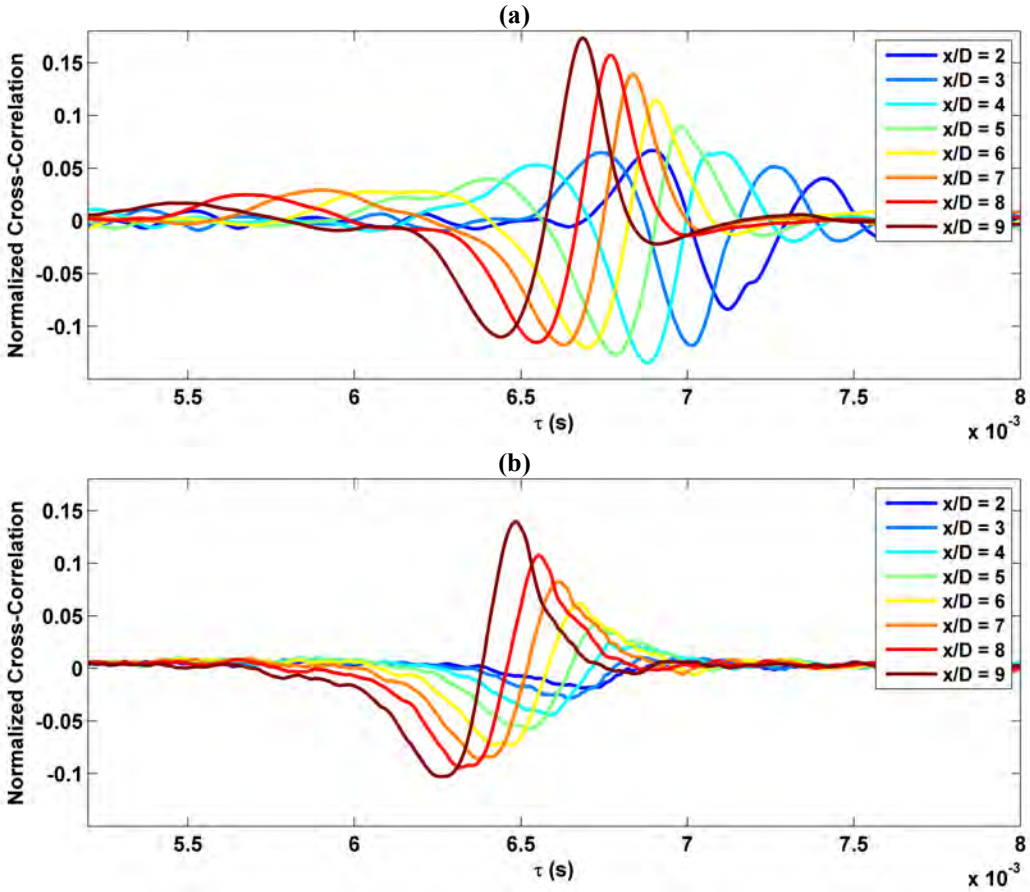

Figure 15. Normalized cross-correlations of the forced instantaneous near-field pressure with the 30° far-field microphone: (a) First array location, (b) Last array location.

In Figure 15, the variation of the normalized cross-correlations of the instantaneous near-field pressure along the first array position (Figure 15(a)) and last array position (Figure 15(b)) with the instantaneous far-field microphone at 30° are presented for the forced jet. Immediately, it is evident from Figure 15 that the cross-correlations for both arrays presented are very similar to the unforced jet (Figure 6). The maximum correlation obtained in Figure 15(a) is approximately 0.17 (compared to 0.2 in the unforced jet). Furthermore, the evolution of the shape of the correlations with downstream displacement is analogous to the unforced jet. The reason for this similarity is probably the very low forcing Strouhal number (0.02) and thus the sparse presence of the structures due to forcing.

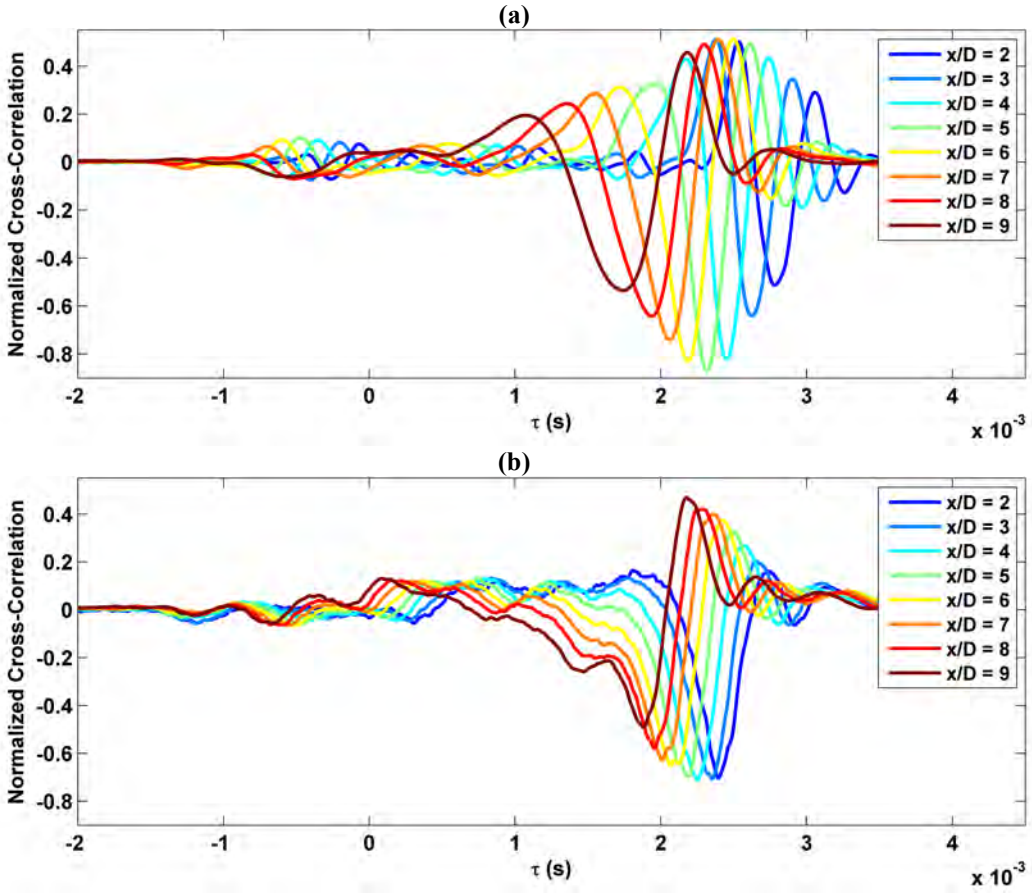

Figure 16. Normalized cross-correlations of the phase-averaged waveform with the 30° far-field microphone: (a) First array location, (b) Last array location.

The downstream variation of the normalized cross-correlations of the phase-averaged near-field and far-field signals along the first array position and last array position with the far-field microphone at 30° are shown in Figure 16(a) and (b), respectively. It is apparent from Figure 16 that the negative peaks are more dominant in both array sets. This differs from the correlations involving the instantaneous signals in the forced jet (Figure 15) as well as the unforced jet (Figure 6), where the positive peaks exhibited higher amplitude. As illustrated in Figure 16(a), the correlation increases as the jet evolves downstream, reaching a maximum of approximately 0.5 (compared to roughly 0.17 in the instantaneous forced case) between x/D = 5 and 8, at which point the correlation decreases slightly. The maximum correlation has also shifted upstream in comparison to the forced instantaneous case and the unforced jet, closer to the end of the potential core. This observation corresponds with the shift seen in Figure 9(b). The downstream evolution of the correlation in Figure 16(b) is similar to that seen in Figure 14(b). Similar to the correlations involving the instantaneous signals in the forced jet, the correlation increases as the jet evolves downstream; however, this sustained growth is only visible for the positive excursions.

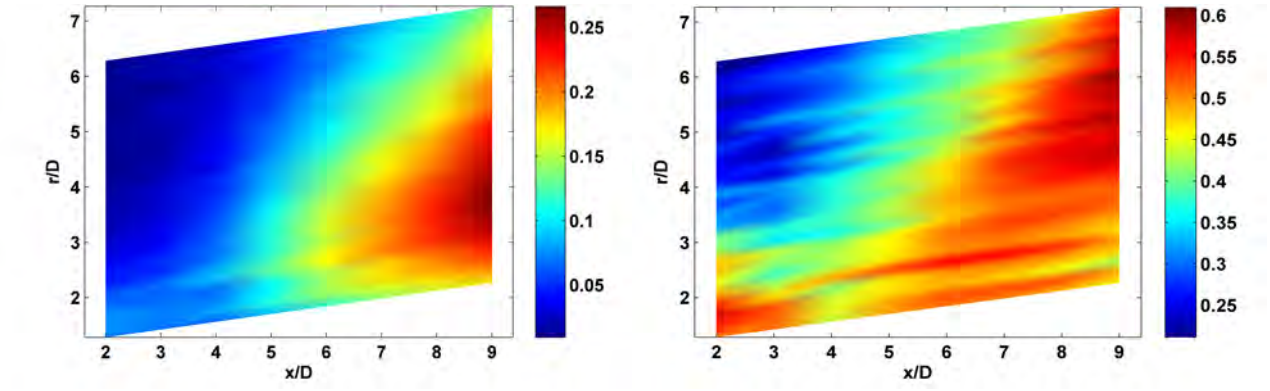

(a) **(b)**

Figure 17. Maximum normalized cross-correlation with the 30° far-field microphone: (a) Filtered instantaneous near-field pressure fluctuations, (b) Filtered phase-averaged waveforms.

Figure 17 shows the maximum normalized cross-correlation to the 30° far field for each microphone location, computed for the forced jet at St_{DF} = 0.02. The values were computed from the instantaneous pressure signals (Figure 17(a)) and the phase-averaged signals (Figure 17(b)) for both the near-field and far-field microphones. Several differences between the two sets of cross-correlations are evident. Figure 17(a) is very similar to the unforced case (Figure 7) apart from slightly higher values upstream. Again, this is due to the very low forcing Strouhal number. On the other hand, the maximum correlation values for the phase-averaged signals (Figure 17(b)) are significantly increased (~0.6 versus ~0.3) over the instantaneous forced signals. The maximum correlation values have also shifted to noticeably higher angles (the angles are measured similar to the Figure 7) for the phase-averaged waveform signals. The upstream, far radial locations still have low correlation to the far field at 30° (relative to the rest of the microphone positions). However, for the region close to the nozzle exit (x/D < 3 and r/D < 2), the correlation values are observed to be unusually high in relation to the surrounding areas.

IV. Conclusions

The response of a high-speed subsonic jet to low-frequency forcing was investigated using localized arc filament plasma actuators (LAFPAs). These actuators have demonstrated strong control authority on high-speed turbulent jets and provide a unique opportunity to study the dynamics of large-scale structures. Eight LAFPAs uniformly arranged around the periphery of the nozzle exit are operated in phase to simulate axisymmetric forcing. The jet Mach number and Reynolds number based on the jet diameter were 0.9 and 6.2×10^5. A traversing linear array which spans eight nozzle exit diameters in the axial direction and five nozzle exit diameters in the radial direction is employed in order to obtain a comprehensive picture of the near hydrodynamic and acoustic fields.

Phase averaging of the pressure signals with respect to the actuator signal was used to separate the relevant features of the response from the background turbulence. The phase-averaged pressure signal of the jet forced at a Strouhal number of 0.02 exhibited a compact sinusoidal wave with a positive excursion preceding a negative excursion; this was demonstrated to be a hydrodynamic response and travelling with the convective speed of the flow structures in the streamwise direction. These hydrodynamic fluctuations were shown to decay rapidly with radial distance. A second compact wave in the phase-averaged pressure waveform, which is of smaller amplitude (in the first array location) and decreased with downstream distance from the nozzle, was shown to be the actuator self-noise traveling with the ambient speed of sound. As the traverse moved radially away from the nozzle, the actuator-self noise became a significant contribution to the overall intensity of the near-field signal. Furthermore, the phase-averaged pressure at the last array location (which is five nozzle exit diameters away from the jet shear layer) mainly constituted a positive excursion. Owing to the growth in amplitude of the actuator noise in the latter array locations, the phase-averaged pressure signal was filtered utilizing a continuous wavelet transform in order to avoid making subsequent analyses difficult to interpret.

Simultaneous measurements of acoustic far field were also performed along with the near field, allowing the relationship between the near-field pressure and the far-field acoustics to be examined. Although the near-field pressure near the jet shear-layer was found to be largely hydrodynamic in nature, there was still significant correlation between that pressure and the far-field acoustic (30° far-field microphone), particularly in the region past the end of the potential core. However, this region shifted upstream closer to the end of the potential core (between x/D = 5 and 8) when the jet was forced at a Strouhal number of 0.02. It is important to note that this trend was

observed for the correlations on the phase-averaged waveforms and do not offer a direct comparison with the unforced jet. The work presented here is preliminary and is currently underway to extend the present analysis by examining the correlations of the axisymmetric jet at different frequencies and over a larger axial domain to determine the effects of forcing further downstream of the end of the potential core.

Acknowledgements

The support of this research by the Air Force Office of Scientific Research with Dr. John Schmisseur is greatly appreciated.

References

1. Jordan, P., and Gervais, Y. "Subsonic Jet Aeroacoustics: Associating Experiment, Modelling and Simulation," *Experiments in Fluids* Vol. 44, No. 1, 2008, pp. 1-21.
2. Samimy, M., Zaman, K. B. M. Q., and Reeder, M. F. "Effect of Tabs on the Flow and Noise Field of an Axisymmetric Jet," *AIAA Journal* Vol. 31, No. 4, 1993, pp. 609-619.
3. Zaman, K. B. M. Q., Reeder, M. F., and Samimy, M. "Control of an axisymmetric jet using vortex generators," *Physics of Fluids* Vol. 6, No. 2, 1994, pp. 778-793.
4. Kim, J.-H., and Samimy, M. "Mixing enhancement via nozzle trailing edge modifications in a high speed rectangular jet," *Physics of Fluids* Vol. 11, No. 9, 1999, pp. 2731-2742.
5. Callender, B., Gutmark, E., and Martens, S. "Far-Field Acoustic Investigation into Chevron Nozzle Mechanisms and Trends," *AIAA Journal* Vol. 43, No. 1, 2004, pp. 87-95.
6. Viswanathan, K. "Nozzle Shaping for Reduction of Jet Noise from Single Jets," *AIAA Journal* Vol. 43, No. 5, 2005, pp. 1008-1022.
7. Crow, S. C., and Champagne, F. H. "Orderly structure in jet turbulence," *Journal of Fluid Mechanics* Vol. 48, No. 3, 1971, pp. 547-591.
8. Kibens, V. "Discrete Noise Spectrum Generated by an Acoustically Excited Jet," *AIAA Journal* Vol. 18, No. 4, 1980, pp. 434-441.
9. Zaman, K. B. M. Q., and Hussain, A. K. M. F. "Vortex pairing in a circular jet under controlled excitation. Part 1. General jet response," *Journal of Fluid Mechanics* Vol. 101, No. 3, 1980, pp. 449-491.
10. Zaman, K. B. M. Q., and Hussain, A. K. M. F. "Turbulence suppression in free shear flows by controlled excitation," *Journal of Fluid Mechanics* Vol. 103, 1981, pp. 133-159.
11. Gutmark, E., and Ho, C.-M. "Preferred modes and the spreading rates of jets," *Physics of Fluids* Vol. 26, No. 10, 1983, pp. 2932-2938.
12. Ho, C.-M., and Huerre, P. "Perturbed free shear layers," *Annual Review of Fluid Mechanics* Vol. 16, 1984, pp. 365-424.
13. Cohen, J., and Wygnanski, I. "The evolution of instabilities in the axisymmetric jet. Part 1. The linear growth of disturbances near the nozzle," *Journal of Fluid Mechanics* Vol. 176, 1987, pp. 191-219.
14. Jendoubi, S., and Strykowski, P. J. "Absolute and Convective Instability of Axisymmetric Jets with External Flow," *Physics of Fluids* Vol. 6, No. 9, 1994, pp. 3000-3009.
15. Samimy, M., Kim, J. H., Kastner, J., Adamovich, I., and Utkin, Y. "Active Control of a Mach 0.9 Jet for Noise Mitigation Using Plasma Actuators," *AIAA Journal* Vol. 45, No. 4, 2007, pp. 890-901.
16. Samimy, M., Kim, J.-H., Kastner, J., Adamovich, I., and Utkin, Y. "Active control of high-speed and high-Reynolds-number jets using plasma actuators," *Journal of Fluid Mechanics* Vol. 578, 2007, pp. 305-330.
17. Jubelin, B. "New Experimental Studies on Jet Noise Amplification," *AIAA 6th Aeroacoustics Conference*. 1980-0961, 1980.
18. Lu, H. Y. "Effect of Excitation on Coaxial Jet Noise," *AIAA Journal* Vol. 21, No. 2, 1983, pp. 214-220.
19. Ahuja, K. K., and Blakney, D. F. "Tone Excited Jets, Part IV: Acoustic Measurements," *Journal of Sound and Vibration* Vol. 102, No. 1, 1985, pp. 93-117.
20. Samimy, M., Kim, J.-H., Kearney-Fischer, M., and Sinha, A. "Acoustic and Flow Fields of an Excited High Reynolds Number Axisymmetric Supersonic Jet," *Journal of Fluid Mechanics* Vol. 656, 2010, pp. 507-529.
21. Kearney-Fischer, M., Kim, J.-H., and Samimy, M. "Control of a high Reynolds number Mach 0.9 heated jet using plasma actuators," *Physics of Fluids* Vol. 21, 2009, p. 095101.
22. Kim, J.-H., Kastner, J., and Samimy, M. "Active Control of a High Reynolds Number Mach 0.9 Axisymmetric Jet," *AIAA Journal* Vol. 47, No. 1, 2009, pp. 116-128.
23. Kearney-Fischer, M., Kim, J.-H., and Samimy, M. "A Study of Mach Wave Radiation Using Active Control," *Journal of Fluid Mechanics* Vol. 681, 2011, pp. 261-292.
24. Kearney-Fischer, M., Kim, J.-H., and Samimy, M. "Noise Control of a High Reynolds Number High Speed Heated Jet Using Plasma Actuators," *International Journal of Aeroacoustics* Vol. 10, No. 5-6, 2011, pp. 635 – 658.

25. Samimy, M., Kim, J.-H., Kastner, J., Adamovich, I., and Utkin, Y. "Active Control of High-Speed and High-Reynolds-Number Jets Using Plasma Actuators," *Journal of Fluid Mechanics* Vol. 578, No. 1, 2007, pp. 305-330.
26. Sinha, A., Kim, K., Kim, J., Serrani, A., and Samimy, M. "Extremizing Feedback Control of a High-Speed and High Reynolds Number Jet," *AIAA Journal* Vol. 48, No. 2, 2010, pp. 387-399.
27. Suzuki, T., and Colonius, T. "Instability waves in a subsonic round jet detected using a near-field phased microphone array," *Journal of Fluid Mechanics* Vol. 565, 2006, pp. 197-226.
28. Tinney, C. E., and Jordan, P. "The near pressure field of co-axial subsonic jets," *Journal of Fluid Mechanics* Vol. 611, 2008, pp. 175-204.
29. Sinha, A., Alkandry, H., Kearney-Fischer, M., Samimy, M., and Colonius, T. "The Impulse Response of a High-Speed Jet Forced with Localized Arc Filament Plasma Actuators," *Physics of Fluids*, to appear, 2012.
30. Arndt, R. E. A., Long, D. F., and Glauser, M. N. "The proper orthogonal decomposition of pressure fluctuations surrounding a turbulent jet," *Journal of Fluid Mechanics* Vol. 340, 1997, pp. 1-33.
31. Coiffet, F., Jordan, P., Oelville, J., Gervais, Y., and Ricaud, F. "Coherent structures in subsonic jets: a quasi-irrotational source mechanism?," *International Journal of Aeroacoustics* Vol. 5, No. 1, 2006, pp. 67 - 89.
32. Hahn, C. "Design and Validation of the New Jet Facility and Anechoic Chamber," M.S. Thesis, *Mechanical Engineering*, The Ohio State Univeristy, 2011.
33. Hahn, C., Kearney-Fischer, M., and Samimy, M. "On factors influencing arc filament plasma actuator performance in control of high speed jets," *Experiments in Fluids* Vol. 37, No. 5, 2011.
34. Hileman, J., Thurow, B., and Samimy, S. "Development and evaluation of a 3-D microphone array to locate individual acoustic sources in a high-speed jet," *Journal of Sound and Vibration* Vol. 276, No. 3-5, 2004, pp. 649-669.
35. Hall, J. W., Pinier, J., Hall, A. e., and Glauser, M. "Two-point correlations of the near and far-field pressure in a transonic jet," *ASME 2006 Joint U.S. European Fluids Engineering Summer Meeting*. FEDSM2006-98458, 2006.
36. Picard, C., and Delville, J. "Pressure velocity coupling in a subsonic round jet," *International Journal of Heat and Fluid Flow* Vol. 21, No. 3, 2000, pp. 359-364.
37. Ukeiley, L. S., and Ponton, M. K. "On the near field pressure of a transonic axisymmetric jet," *International Journal of Aeroacoustics* Vol. 3, No. 1, 2004, pp. 43-66.